



# Reinforcing and Toughening Modification of poly (3-hydroxybutyrate-co-3-hydroxyvalerate)/ethylene-vinyl Acetate Copolymer (PHBV/EVA) Blends Compatibilized by Benzoyl Peroxide

Yiqi Fang<sup>1,2</sup> · Yansong Huang<sup>1,2</sup> · Jiawei Huang<sup>1,2</sup> · Yujuan Jin<sup>1,2</sup> · You Wu<sup>1,2</sup> · Huafeng Tian<sup>1,2</sup> · Xiaojuan Zhang<sup>1,2</sup>

Accepted: 31 August 2023 / Published online: 14 September 2023

© The Author(s), under exclusive licence to Springer Science+Business Media, LLC, part of Springer Nature 2023

## Abstract

Due to the high brittleness of poly (3-hydroxybutyrate-co-3-hydroxyvalerate) (PHBV), ethylene-vinyl acetate copolymer (EVA) was incorporated to prepare PHBV/EVA blends by melt blending, and the compatibility of the blends was improved by benzoyl peroxide (BPO). The research found that the addition of BPO triggered the production of free radicals in the PHBV and EVA polymers, followed by the recombination of the radicals to form the chemical cross-linking. The resultant PHBV/EVA/BPO blends showed improved mechanical properties and compatibility. At the optimal BPO content (0.5 phr), the elongation at break increased from 1.24% to 4.47%, the impact strength increased from 7.50 kJ/m<sup>2</sup> to 17.75 kJ/m<sup>2</sup>, and the tensile toughness increased from 15.96 MJ/m<sup>3</sup> to 70.00 MJ/m<sup>3</sup>. The gel content of the blends also reached the maximum value (13.88%) at 0.5 phr of BPO addition. This improvement was primarily attributed to interfacial adhesion between PHBV and EVA due to the chemical cross-linking, the hydrogen bonding interactions and the blends chain entanglements. Therefore, this research can improve the poor mechanical properties of PHBV and expand its potential application value.

**Keywords** Poly (3-hydroxybutyrate-co-3-hydroxyvalerate) (PHBV), Benzoyl peroxide (BPO), Ethylene-vinyl acetate copolymer (EVA) · Interfacial adhesion · Chemical cross-linking

## Introduction

In recent years, significant efforts have been made to solve the plastic pollution through the replacement of petroleum-based polymers with bio-based polymers [1, 2]. Bio-based plastics exhibit high performance with significantly lower

carbon emissions and energy production requirements compared to fossil-based plastics [3, 4]. Among the bio-based and biodegradable plastics, polyhydroxyalkanoates (PHAs) are a special family of polymers that have attracted considerable attention due to their biocompatibility, biodegradability and the ability to use a range of different renewable and waste-based feedstocks to produce them [5–7].

In PHAs family, poly(3-hydroxybutyrate-co-3-hydroxyvalerate) (PHBV) is a thermoplastic polyester with applications in many fields including food, biomedical, cosmetic, electronic packaging and so on [8, 9]. However, PHBV is brittle and stiff with weak mechanical properties. So far, the application of PHBV-based materials is limited because their brittleness, unfavorable thermal stability during processing and a low crystallization rate resulting in aging after shaping [10]. Several efforts had been made to improve the properties of PHBV and overcome the challenges posed by applications, including addition of plasticizers, nucleating agents or blending with other flexible polymers [11–13].

✉ Yujuan Jin  
jinyujuan@th.btbu.edu.cn

✉ Huafeng Tian  
tianhuafeng@th.btbu.edu.cn

✉ Xiaojuan Zhang  
zhxiaojuan@btbu.edu.cn

<sup>1</sup> School of Chemistry and Materials Engineering, Beijing Technology and Business University, Beijing 100048, P. R. China

<sup>2</sup> Beijing Key Laboratory of Quality Evaluation Technology for Hygiene and Safety of Plastics, Beijing Technology and Business University, Beijing 100048, P. R. China

Adding elastomeric materials is an effective way to improve the mechanical properties of brittle plastics [14]. Among the elastomeric materials, ethylene–vinyl acetate copolymer (EVA) is maturely developed and used in the modification studies [15, 16]. Daisuke Kugimoto et al. [17] investigated the effect of EVA on the rheological properties of poly (lactic acid) (PLA). Due to its long-chain branching structure and strain hardening, EVA improved the processability and the mechanical toughness of PLA.

In addition, mechanical property improvement after blending is severely limited by the compatibility between different polymers. Some studies [5, 11, 12, 18] have found that blending with EVA improves the toughness of PHBV to some extent, but it is associated with a loss of tensile strength due to their incompatibility. Therefore, it is imperative to increase the compatibility of PHBV/EVA to further improve its performance. Peroxide additives are a frequently used class of reactive additives that generate free radicals and initiate crosslinking along with grafting reactions [19, 20]. Hu et al. [21] modified poly (butylene succinate) (PBS)/PLA blends using BPO as cross-linking agent. The addition of BPO induced chemical cross-linking reaction between PBS and PLA and improved the interfacial interactions for PBS/PLA blends. Yan et al. [22] prepared PBS/waxy starch (WS)/BPO composites by an internal mixer. A crosslinked graft copolymer (WS-g-PBS) is created by melt blending with BPO, which improved the mechanical properties of the composites and compatibility between PBS and WS.

In this work, BPO was chosen as a cross-linking agent to improve the compatibility of PHBV/EVA and the effect of BPO content on the compatibility PHBV/EVA was investigated. The results indicated that the incorporation of BPO triggered the chemical cross-linking between PHBV and EVA, improving the compatibility and mechanical properties of PHBV/EVA.

## Experimental Section

### Materials

PHBV (Y1000P,  $M_w = 3.00 \times 10^5 \text{ g} \cdot \text{mol}^{-1}$ , the molar content of HV is 3.00%) was supplied by Ningbo Tian'an Biological Co., Ltd. EVA (LEVAPREN 500, the weight% of VA is 50.00%) was purchased from LANXESS Chemical Corporation. Chloroform (Analytical reagent) was purchased from Beijing Chemical Works. Benzoyl peroxide (BPO) (Analytical reagent,  $M_w = 242.23 \text{ g} \cdot \text{mol}^{-1}$ ) were obtained from Shanghai Maclin Biochemical Technology Co., LTD.

### Preparation of the Blends

Before preparation, PHBV was dried for 4 h at 70 °C and EVA was dried for 8 h at 40 °C under vacuum (DZG-6050, Shanghai Sumsung Laboratory Instrument Co., Ltd.). PHBV/EVA blends were prepared by melt blending at a ratio of 8:2 using a twin-screw extruder (CTE-35, L/D ratio is 42/1, Cobelon Coya Machinery Co., Ltd) in presence of different amounts of BPO (0, 0.3, 0.5, 0.7 and 2 phr). The temperature of each zone was set to 165 °C, 165 °C, 168 °C, 168 °C and 170 °C, while the rotational speed was 60 r/min. After the samples were cooled down, the granulator (HP-150, Beijing Huanya Tianyuan Mechanical Technology Co., Ltd.) was used to pelletize the samples; The injection molding machine (TY400, HangZhou DaYu Machinery Co., Ltd.) was used to prepare the sample strips with injection pressure of 4.8 MPa, injection volume of 18%, and the temperature of each zone is 165 °C. The holding pressure is 75 bar, the holding time is 30s and the cooling time is 5s of the injection molding machine. The screw diameter is 18 mm and the L/D ratio is 20.

### Characterization

Fourier-transformed infrared spectroscopy (FT-IR) spectra were obtained by a Nicolet iZ10 (Thermo scientific, USA). PHBV/EVA/BPO blends were prepared by using KBr compression method.

In circulating system, the samples were dissolved by heating reflux in chloroform at 60 °C for 8 h. Then they were removed and dried at 80 °C for 4 h. The gel content was calculated according to Eq. 1. Where  $m_1$  and  $m_2$  represented the mass of the samples after and before dissolution, respectively.

$$a = \frac{m_1}{m_2} \times 100\% \quad (1)$$

The tensile properties were tested using a universal testing machine (CMT604, MTS Industry System Co., Ltd., Guangdong, China) with a set tensile rate of 5 mm/min, a load of 10 kN, and a sample size was established according to the ISO 527-2:2012 standard (dumbbell shaped specimen, L=150 mm, d=4 mm). According to the ISO 180:2000 standard, the sample was subjected to an impact test using the electronic Izod impact testing equipment (XJUD-5.5, Chengde Jinjian Testing Instrument Co., Ltd., Hebei, China). A 1 J energy pendulum test was used to test the notched sample. Five times for each sample was repeated, and the average value of elongation at break, tensile strength and impact strength were recorded.

Scanning electron microscope (SEM) (QUATA250, FEI, USA) operating at 10 kV accelerating voltage was used to observe the impacted fracture surface of samples. Prior to observation, gold spraying was performed at an operating voltage of 15 kV.

Rheological test was conducted by using a Rotary Rheometer (MARS, Thermo Scientific Co., Ltd.) at 180°C. The angular velocity was adjusted from 0.01 to 100 rad/s.

A small number of samples was placed on two slides on a hot table and pressed into thin slices. The sample was heated to 200 °C at a heating rate of 50 °C/min, held for 3 min and then cooled naturally to room temperature. A polarizing microscope (POM) (CBX51, Olympus, Japan) was used to observe crystal growth images during cooling and spherulitic morphology.

The melting and non-isothermal crystallization of the blends were carried out by differential scanning calorimetry (DSC) (Q20, TA Instruments, USA). Firstly, the blends were melted at 200 °C for 3 min and then cooled to -50 °C and then reheated to 200 °C at 10 °C/min. The degree of crystallinity ( $X_c$ ) of the blends was calculated using Eq. (2):

$$X_c = \frac{\Delta H_m}{w \bullet \Delta H_m^0} \times 100\% \quad (2)$$

where  $\Delta H_m$  is the melting enthalpy,  $w$  is the percentage of PHBV in the blends,  $\Delta H_m^0$  is the melting enthalpy of pure PHBV ( $\Delta H_m^0 = 146.6 \text{ J} \cdot \text{g}^{-1}$ )

Thermogravimetric analyses were performed under nitrogen atmosphere in a thermal stability analysis (TGA) (Q50, TA Instruments, USA). Approximately, the samples were heated from room temperature to 600 °C with a heat rate of 20 °C·min<sup>-1</sup>.

## Results and Discussion

### Chemical Structure and Interactions

The FTIR spectra of pure PHBV, EVA and PHBV/EVA/BPO were shown in Fig. 1(a). The characteristic wide absorption peaks of -OH group stretching vibration appeared at 3436 cm<sup>-1</sup>. The bands near 2976, 2933 and 2850 cm<sup>-1</sup> corresponded to -CH<sub>3</sub> and -CH<sub>2</sub> stretching vibrations. The peaks at 1725 cm<sup>-1</sup> and 1622 cm<sup>-1</sup> were attributed to C=O vibration. Compared with neat PHBV and EVA, the PHBV/EVA blends exhibited a relatively strong C=O peak. After adding BPO, the O-H peak of PHBV/EVA/BPO blends was enhanced and the bandwidth of the peak was broadened. It was clear that no new chemical bonds formed in the blends, but the carbonyl groups changed significantly. The peak of C=O groups at 1622 cm<sup>-1</sup> was present in PHBV/EVA/BPO

blends, the polarity of carbonyl groups was weakened. This was ascribed to the formation of intermolecular hydrogen bonding between PHBV hydroxyl groups and EVA carbonyl groups and thus resulting in a leftward shift of the C=O band [23].

To confirm the formation of the chemical cross-linking structure, the gel content of the PHBV/EVA/BPO blends was measured. During the dissolving process, physical cross-linked molecular chains are completely dissolved due to the rupture of hydrogen bonds. In contrast, the molecular chains with chemical cross-linking can only be swelled [24]. The specific gel content was shown in Fig. 1(b). It was obvious that the gel content increased with increasing concentration of BPO but reached a plateau at a BPO concentration of 0.5 phr. The gel content of the PHBV/EVA blends was only 0.77%. When the content of BPO was 0.5 phr, the degree of chemical cross-linking was about 13.88%. However, the gel content of PHBV/EVA/BPO declined after reaching the maximum value at 0.5 phr BPO. This was due to the fact that excessive BPO amount tended to cause chain breakage of PHBV and the gel content decreased as a result.

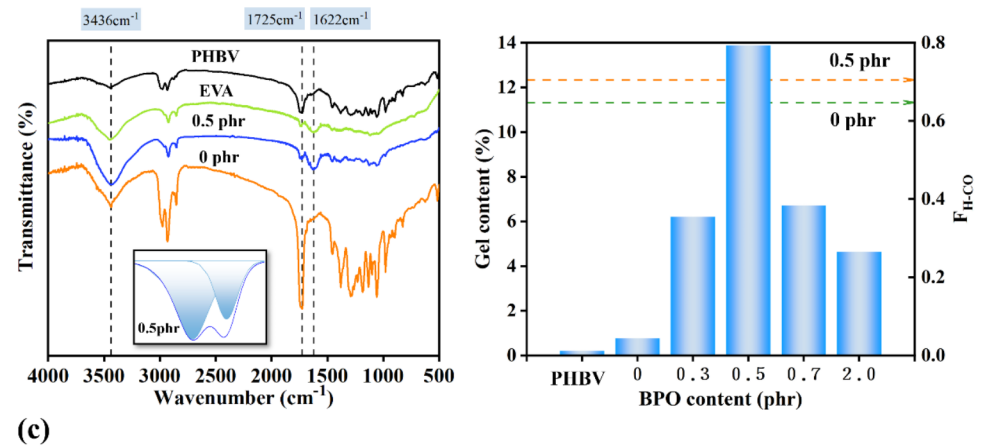
Figure 1(c) displayed the cross-linking reaction mechanism and the hydrogen bonding interaction of the blends. Generally speaking, the BPO produced primary free radicals (RO·) among thermal decomposition. Then the free radicals of tertiary carbon of PHBV and EVA reacted with “RO·” to link the different polymer chains, resulting in carbon-carbon crosslinking reaction [25–29]. At the same time, the hydroxyl group of PHBV interacted with the carbonyl groups in EVA to form hydrogen bonds. The formed chemical cross-linking structure contributed to enhance hydrogen bonding interaction between PHBV and EVA.

In order to determine the hydrogen bond fraction ( $F_{H-CO}$ ), the FTIR spectra of the carbonyl band (1680 to 1800 cm<sup>-1</sup>) were fitted to a curve using the Gaussian-Lorentz spectral function. To further analyze the change of hydrogen bonding interaction in the blends,  $F_{H-CO}$  values can be calculated by the following Eq. (3) [30].

$$F_{H-CO} = \frac{A_H/r_{H/a}}{(A_H/r_{H/a} + A_a)} \quad (3)$$

where  $r_{H/a}$  is the absorption ratio of the above two bands (1.25~1.75),  $A_H$  and  $A_a$  are the hydrogen bonded and carbonyl group free peak areas, respectively. For the present study,  $r_{H/a}$  has been set at 1.35 for semiquantitative comparisons, depending on the hydrogen bond strength. The  $F_{H-CO}$  values of the blends was shown in Fig. 1(b). It could be seen that the  $F_{H-CO}$  of the blends with 0.5 phr BPO was relatively strong, indicating the enhanced hydrogen bonding interactions which resulted from the improved chemical cross-linking between PHBV and EVA in the presence of BPO.

**Fig. 1 (a).** FTIR analysis of the pure PHBV, EVA and PHBV/EVA/BPO blends and peak deconvolution for 0.5 phr BPO (inset), **(b).** Gel content and  $F_{H-CO}$  of PHBV/EVA/ BPO blends, **(c).** Reaction mechanism and Hydrogen bonding interaction of the PHBV/EVA/BPO blends



## Mechanical Properties

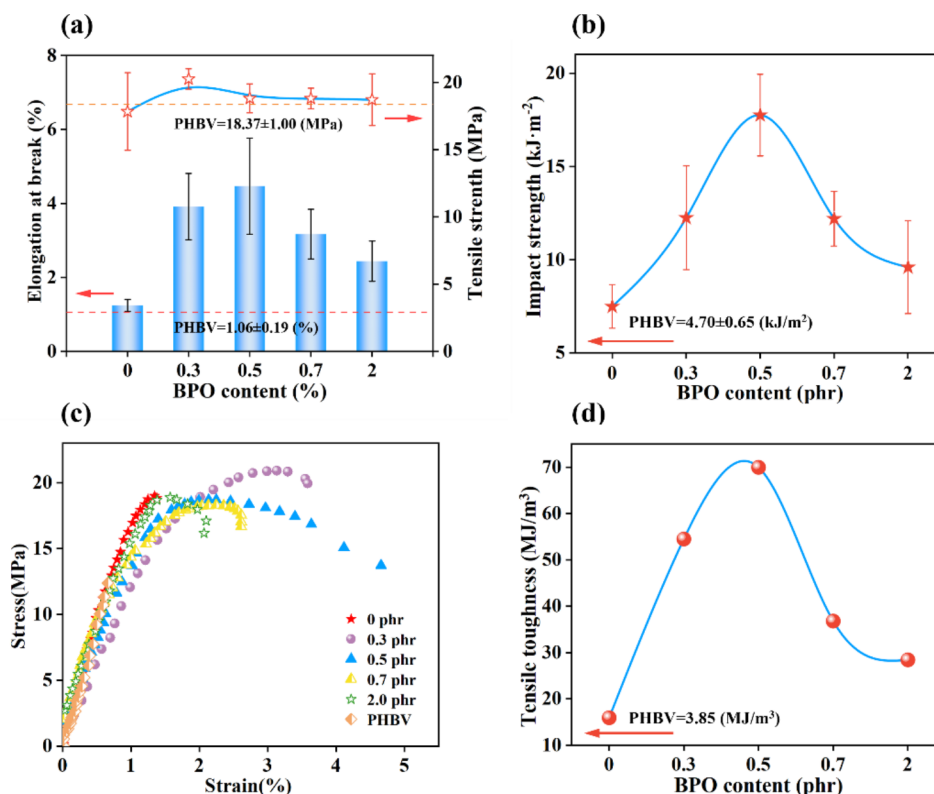
The mechanical properties of the PHBV/EVA and PHBV/EVA/BPO blends with different BPO contents were shown in Fig. 2. The tensile strength of the blends increased and then decreased slightly with the addition of BPO (Fig. 2a). The tensile strength of the blends with 0.3 phr BPO was increased by 14.00% compared to the PHBV/EVA blends. Meanwhile, the elongation at break (Fig. 2a) increased substantially and reached a maximum at a BPO content of 0.5 phr, which were increased by 360.48% than that of PHBV/EVA blends. These were attributed to the chemical cross-linking and hydrogen bonding between PHBV and EVA when BPO was added to the blends. This led to the molecular chains of the blends curlier and longer, resulting in more chain entanglement and limiting chain movement [30, 31]. In the process of the chemical bonds and hydrogen bonds

disruption, the chains required more interfacial slip and broke more entanglement. It was evident that good reinforcing and toughening effect could be achieved by adding BPO into the blends.

The impact strength of the PHBV/EVA/BPO blends initially increased and then declined with the increasing BPO, as shown in Fig. 2(b). The impact strength of the blends with 0.5 phr BPO was increased by 137.30%, from 7.50 kJ/m<sup>2</sup> of the PHBV/EVA blends to 17.80 kJ/m<sup>2</sup>. After adding BPO, the chemical cross-linking between PHBV and EVA produced new chemical bonds and enhanced the interfacial adhesion, resulting in the polymer chains required a higher amount of energy to rupture the material.

Figure 2(c) depicted the stress-strain curves of the blends. The tensile toughness was the integral area under the stress-strain curve (Fig. 2d). The tensile toughness possessed a similar trend with the impact strength. When the content of BPO exceed 0.5 phr, the impact strength, the tensile

**Fig. 2** Mechanical properties test results of the pure PHBV and PHBV/EVA/BPO blends. **(a)** elongation at break and tensile strength, **(b)** impact strength, **(c)** stress-strain curve, **(d)** tensile toughness.



toughness and the elongation at break of the blends showed a downward trend. The slight agglomeration of BPO was mainly responsible for this, which could be supported by the SEM observation. Thus, 0.5 phr BPO was found to give the best mechanical properties of the blends.

## SEM

The impact fracture morphology of the pure PHBV and PHBV/EVA/BPO ternary blends was shown in Fig. 3 (a-f). The pure PHBV displayed a typical brittle fracture, presenting a smooth impact surface (Fig. 3a). After the addition of EVA, the blends exhibited rougher interface with a large area of stress whitening (Fig. 3b). A significant interphase gap was observed between the EVA elastomer and PHBV, due to the poor compatibility between the two polymers. The EVA elastomer underwent brittle pull-out and debonded from the PHBV without sufficient deformation and dislodges from the PHBV, due to their poor adhesion to the PHBV interface, forming microvoids (the red circle). After adding BPO, the rough structures gradually became unclear and the interface became blurred. The rubbery EVA was also more homogeneously distributed in the PHBV matrix, indicating that the compatibility between the two phases had been increased. By comparing Fig. 3 (b-f), it was found that the observation of the microvoids and the brittle pull-out phenomenon were not obvious for the PHBV/EVA blends with BPO. The

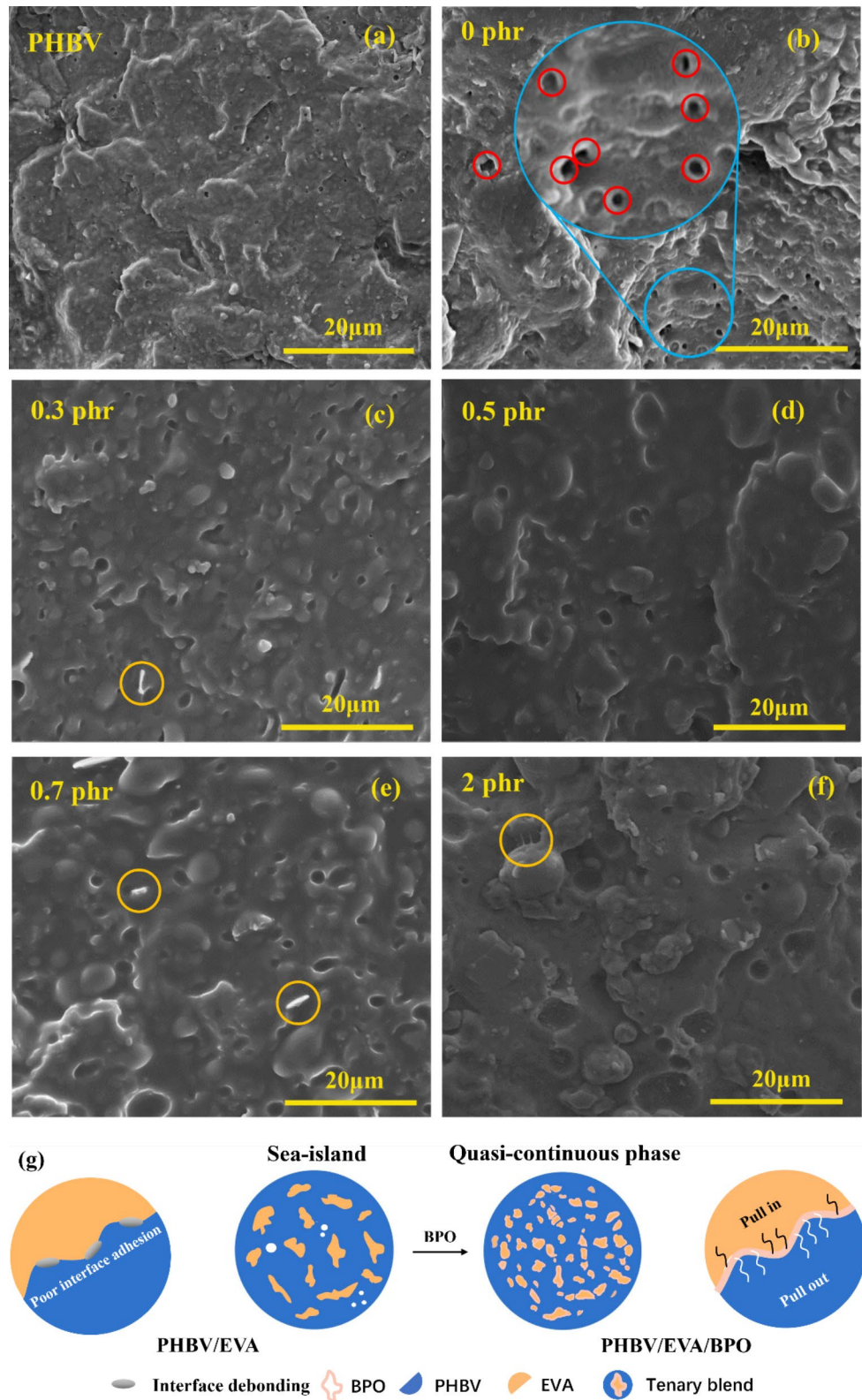
addition of BPO resulted in the formation of chemical cross-linking and stronger interfacial adhesion between the PHBV and EVA. Also, the enhanced interfacial interaction led to yield deformation and fibre formation (the yellow circle) during the process of pull-out. The high interfacial adhesion and cavitation of the elastomer are highly beneficial for improving the toughness [32].

The above toughening interfacial mechanism was also displayed in Fig. 3(g). BPO transformed the morphology of the ternary blends into quasi-continuous phase structure by chemical cross-linking. Therefore, a large amount of the fractured energy was dissipated that led to achieve toughening performance.

## Rheological Analysis

To understand the compatibility of blends and the toughening mechanism, it was important to analyze the rheological behavior of blends. The viscosity ( $\eta^*$ ), the storage modulus ( $G'$ ) and loss modulus ( $G''$ ) of PHBV/EVA/BPO blends as a function of angular frequency ( $\omega$ ) were shown in Fig. 4. The viscosity of the PHBV/EVA/BPO blends decreased sharply with the increment of frequency and then flattened (Fig. 4a). However, the viscosity of PHBV/EVA blends was not significantly related to frequency during long-term motion due to the lack of chain entanglement. After the addition of BPO, the viscosity gradually increased and

**Fig. 3** SEM image of the impact section of pure PHBV and PHBV/EVA/BPO blends. **(a)** pure PHBV, **(b)** 0 phr, **(c)** 0.3 phr, **(d)** 0.5 phr, **(e)** 0.7 phr, **(f)** 2 phr, **(g)** The possible interfacial mechanism for PHVB/EVA/BPO blends



reached a maximum at 0.5 phr BPO. In ternary blends, the addition of benzoyl peroxide not only increased the chain entanglement in the blends, but also enhanced the interfacial adhesion between PHBV and EVA. This was due to the

fact that BPO triggered the chemical cross-linking reaction between PHBV and EVA, resulting in the long molecular chains more tightly intertwined at the beginning of shear. Therefore, the introduction of BPO significantly improved

the loss modulus and storage modulus of the blends, higher than those of neat PHBV/EVA in Fig. 4b and c.

In addition, the relaxation process can be described by the Cole-Cole semicircle (Fig. 4d) to verify the compatibility between PHBV and EVA. The Cole-Cole plot was obtained by plotting the real part ( $\eta'$ ) and the imaginary part ( $\eta''$ ) of the complex dielectric function in the low-energy-loss region. In general, a smooth, half-round shape of the plotted curves indicates a high degree compatibility and phase homogeneity in the melt. On the contrary, any deviation from this shape exhibits a non-homogeneous dispersion and phase segregation due to incompatibility [33–35]. In this way, the extent of compatibility between PHBV and EVA could be effectively evaluated. As can be seen from the smooth semi-circular shape of the plots (yellow dashed line), the mixtures with 0.5 phr BPO show the most homogeneous dispersion. The deviation from the semicircular shape was more obvious for PHBV/EVA blends than for the blends with BPO. As mentioned above, the compatibility of PHBV/EVA blends was highly improved by the addition of BPO.

## POM

The POM images of the blends were shown in Fig. 5(a–f). Figure 5(a) showed the dimension of PHBV spherulite

was large. However, a small number of intact spherical crystals can be seen in Fig. 5(b), with the blurred outline of PHBV ring Maltese cross spherulites. This is due to the poor compatibility between PHBV and EVA. The pure blends exhibited two different crystal topographies, where the incomplete spherulite PHBV crystals were hindered by the EVA phase. After the addition of BPO, the size of the PHBV crystals was gradually become large and the size of the EVA domain decreased, but defects still existed inside the crystal (Fig. 5c). With the addition of BPO up to 0.5 phr, the crystal topography separation was decreased. Moreover, the defects inside of spherical crystal seemed to be more uniformly distributed and the flake Maltese cross of PHBV spherulites displayed, as shown in Fig. 5(d). Furthermore, the blends with 0.7 phr and 2.0 phr BPO, the spherulite size increased and the spherulite density decreased (Fig. 5e and f), an indication of BPO agglomeration leading to reduced nucleation sites and increased chain diffusion. In line with previous studies, BPO could improve the compatibility of PHBV and EVA by chemical cross-linking.

Dynamic competition theory can explain these results [36, 37] in Fig. 5(g). The Elastomers phase or BPO cross-linking agents restricted further growth of PHBV crystals. Meanwhile, BPO wrapped on EVA surface increased inter-chain interactions to promote their crystallization ability and form more perfect spherulites.

**Fig. 4** Rheology analysis of PHBV/EVA/BPO blends (a)  $\eta^*$ , (b)  $G'$ , (c)  $G''$ , (d) the Cole-Cole semicircle

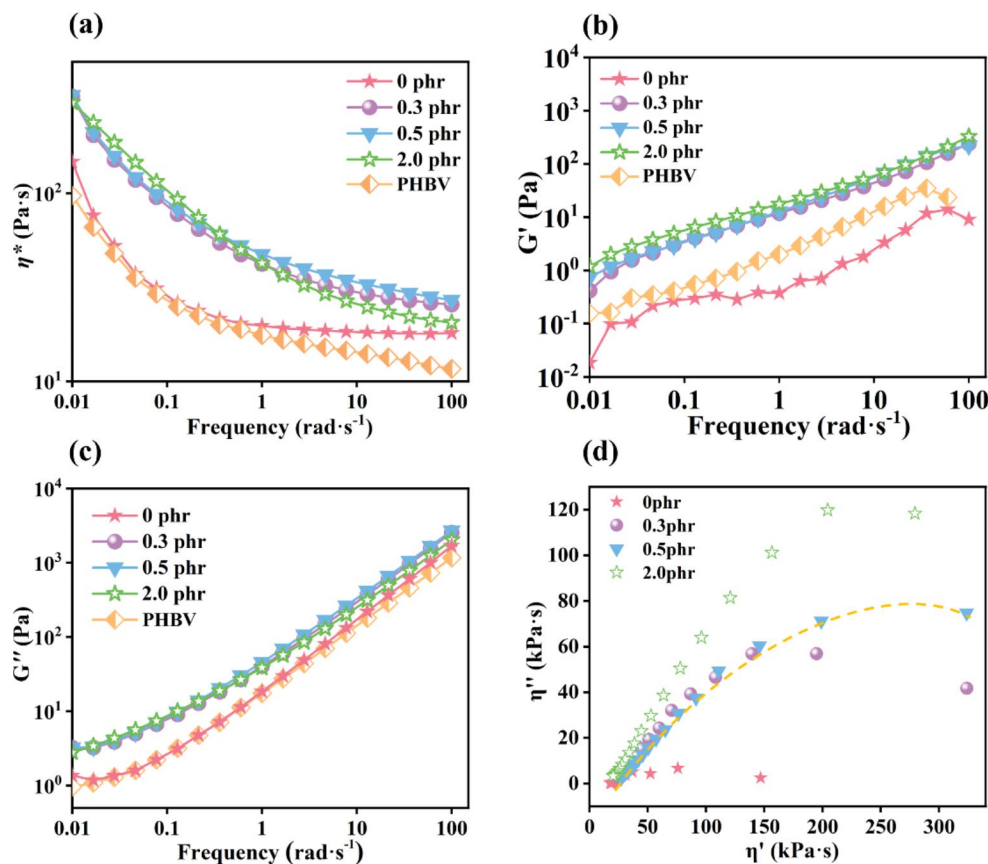


**Fig. 5** Polarization diagram of the PHBV and PHBV/EVA/BPO blends. (a) pure PHBV; (b) 0 phr; (c) 0.3 phr; (d) 0.5 phr; (e) 0.7 phr; (f) 2 phr. (g) dynamic competition mechanism of PHBV with EVA and BPO

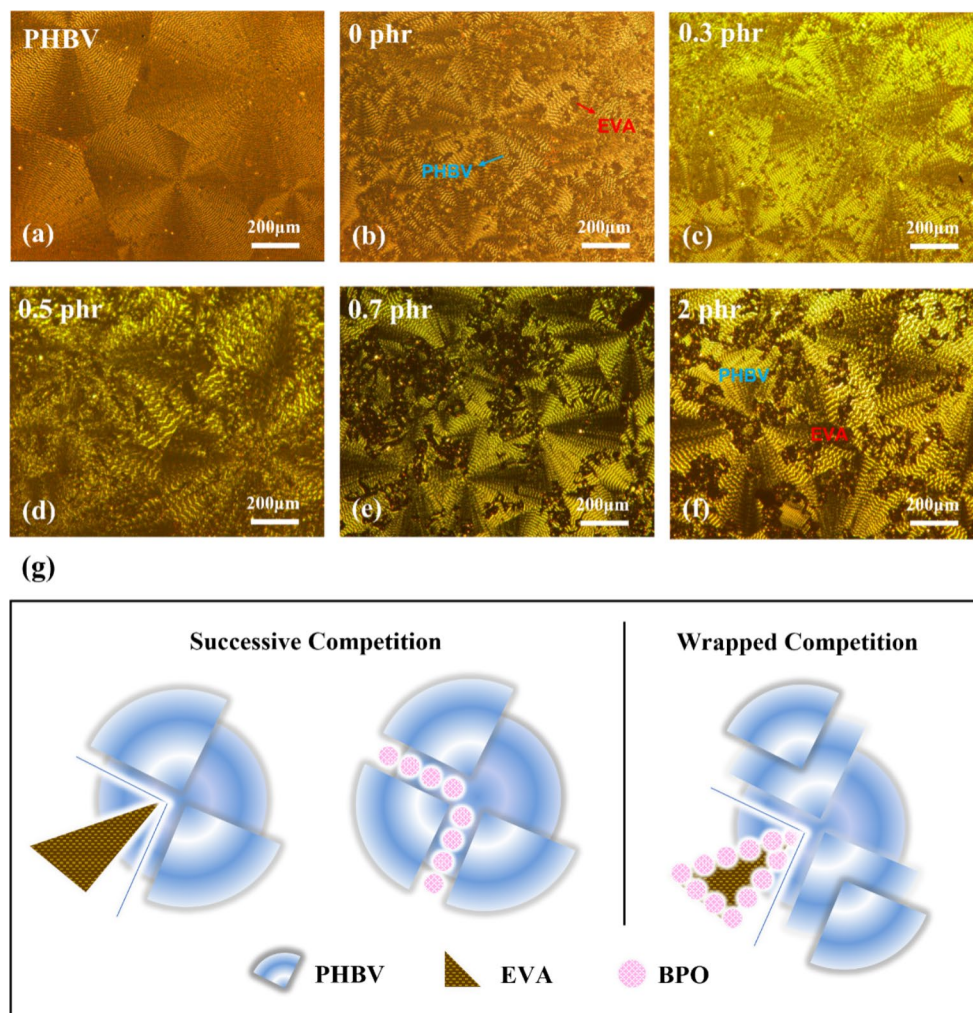


**Table 1** Thermal parameters from DSC and TGA characterizations

BPO content(phr)	$T_c$ (°C)	$\Delta H_c$ (J/g)	$T_m$ (°C)	$\Delta H_m$ (J/g)	$X_c$ (%)	$T_{5\%}$ (°C)	$T_{max}$ (°C)	$E_t$ (kJ/mol)
PHBV	106.4	71.3	172.3	80.1	54.9	265.5	289.3	/
0	107.8	85.9	168.2	108.0	59.2	290.8	304.1	132.89
0.3	105.5	71	167.9	88.9	48.7	278.0	296.1	110.69
0.5	104.6	58.7	166.3	75.4	41.3	285.5	299.3	136.84
0.7	104.4	66.3	166.9	86.2	47.3	287.0	303.4	124.28
2	101.6	62.4	167.6	81.2	44.5	277.6	292.9	111.39

## Thermal Properties

To analyze the effect of BPO concentration on the crystallization behaviors, DSC for the pure PHBV and PHBV/EVA/BPO blends as shown in Fig. 6a-b and the thermal parameters were given and Table 1. The crystallinities ( $X_c$ ) decreased from 59.2% of PHBV/EVA blends to 41.3% of PHBV/EVA/BPO (0.5phr). There were two main reasons for this phenomenon. On the one hand, the formation of chemical cross-linking structures in the melt state (amorphous phase) disturbed the reorganization and chain folding during crystallization process, which would result in the

formation of imperfect crystallite with smaller size. On the other hand, the formation of chain entanglement between PHBV and EVA limited the mobility of PHBV/EVA blends chains, leading to incomplete crystals and reduced crystallinity. The endothermic melting peak with a high temperature shoulder were observed at 170°C for the blends was shown in Fig. 6b. The occurrence of multiple peaks in PHBV blends has been reported in the following literatures [5, 38–40]. The reason for this phenomenon was that the incomplete crystallite formed during the cold crystallization process can be melted and re-crystallized as the



temperature rises, while at higher temperatures, the crystals melt completely.

In addition, the crystallization enthalpy ( $\Delta H_c$ ), the melting temperature ( $T_m$ ) and the melting enthalpy ( $\Delta H_m$ ) of PHBV/EVA mixture showed a declining trend, reaching the lowest value when the BPO content was 0.5 phr. This phenomenon was caused by the increased crosslink density through aggrandizing the addition of peroxide, leading to reduce the degree of crystallinity of the blends. Crosslinks acted as defect centers, hindering the folding of the macromolecular chains and thus reducing the sizes of the crystals [41]. The endothermic melting peak with a high temperature shoulder was most pronounced at PHBV/EVA blends with 0.5phr BPO, because the degree of chemical cross-linking reached its maximum value. The formation of chemical cross-linking structures disturbed the reorganization and chain folding during crystallization process, which would result in the formation of imperfect crystallite.

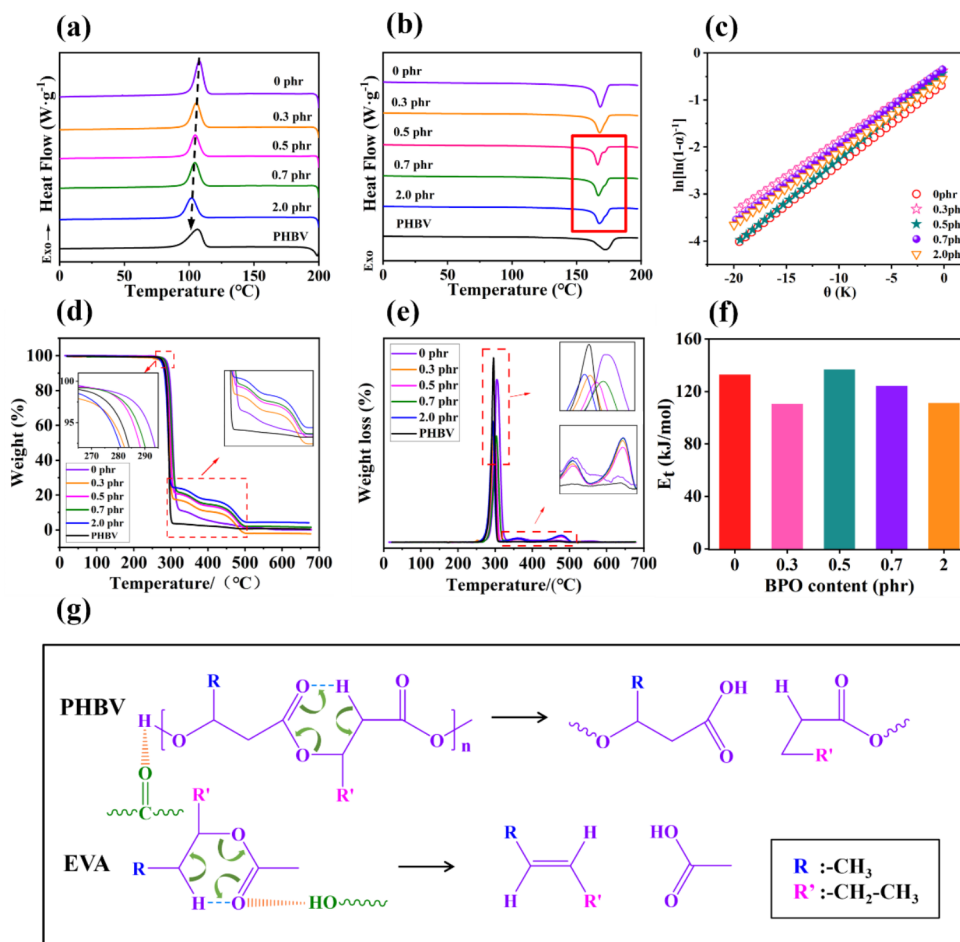
Figure 6 (d) and (e) show the TGA and DTG curves of PHBV/EVA/BPO blends. The blends evidenced a two-stage weight loss. The weight of 250°C–300°C was attributed to the PHBV degradation, and that of 300°C–500°C was attributed to the degradation of EVA. Compared with pure

PHBV/EVA, the initial decomposition temperature ( $T_{50\%}$ ) and the maximum decomposition temperature ( $T_{max}$ ) of PHBV/EVA/BPO decreased slightly. It was due to the fact that the chemical cross-linking between PHBV and EVA limited the mobility of the blends chains and imperfect crystals formed. The reason for above phenomenon also could be explained by the mechanism of thermal degradation of PHBV and EVA, as shown in Fig. 6(g) [42–44]. The addition of BPO promoted hydrogen bonding, but the hydrogen bonding interactions did not affect the development of the six-membered ester ring during the degradation of PHBV. However, hydrogen bonding interactions might prevent the formation of a six-membered ester ring during the thermal degradation process of EVA, thereby increasing its thermal stability.

Using the integral method proposed by Horowitz and Metzger, the activation energy ( $E_a$ ) of the blends with different BPO contents can be calculated from the TGA curves. The equation derived by Horowitz-Metzger is as follow [45, 46]:

$$\theta = T - T_{max} \quad (5)$$

**Fig. 6** Thermal performance of the PHBV/EVA/BPO blends. **(a)**. DSC curve of cooling process, **(b)**. DSC curve of secondary heating, **(c)**. Flow activation energies, **(d)**. Thermal weight loss curve, **(e)**. Thermal weight loss rate curve, **(f)**. Plots of  $\ln[\ln(1-\alpha)^{-1}]$  vs.  $\theta$  for determination of the decomposition activation energy. **(g)**. The general mechanism of thermal degradation of PHBV and EVA



$$\ln \left[ \ln (1 - \alpha)^{-1} \right] = \frac{E_t \theta}{RT_{max}^2} \quad (6)$$

where  $T_{max}$  is the temperature at the maximum rate of weight loss,  $\alpha$  is the decomposed fraction of the sample,  $E_t$  is the activation energy for decomposition, and  $R$  is the gas constant. A plot of  $\ln \left[ \ln (1 - \alpha)^{-1} \right]$  versus  $\theta$  can yield activation energy ( $E_t$ ). (Fig. 6c and f). It was easily seen that the addition of BPO decreased the  $E_t$  of the blends, but there was a small improvement in the activation energy when the BPO content was 0.5 phr. In a word, the formation of chemical cross-linking structures between PHBV and EVA had little effect on the thermal stability of the PHBV/EVA/BPO blends.

## Conclusions

In this work, BPO was chosen as a cross-linking agent to improve the compatibility of PHBV/EVA. It was found that the addition of BPO could effectively improve the compatibility and toughness of PHBV/EVA blends. The addition of BPO to the blends triggered the chemical cross-linking reaction of PHBV and EVA, as indicated by the gel content. The FT-IR spectra revealed the hydrogen bonding interaction occurred in the blends was enhanced by the chemical cross-linking reaction. When 0.5 phr BPO was added, the distribution of defects inside the spherical crystals was more uniform and the crystallinity decreased to 41.3%. Furthermore, the elongation at break and impact strength of PHBV/EVA/BPO blends reached the highest, increasing 260.2% and 136.7%, respectively, compared with those without BPO addition. The compatibilized and toughened PHBV/EVA/BPO blends with melt elasticity and excellent mechanical properties are expected to find widespread use in future packaging applications.

**Acknowledgements** The authors are grateful to the support of National Natural Science Youth Foundation (51503007), Beijing Key Laboratory of Quality Evaluation Technology for Hygiene and Safety of Plastics (QETHSP2020013).

**Author Contributions** Yiqi Fang wrote the main manuscript text, designed of methodology and analysed data. Yansong Huang reviewed the manuscript and verified experimental design. You Wu verified experimental design and did data Curation. Yujuan Jin, Huafeng Tian and Xiaojuan Zhang reviewed and edited the manuscript.

**Funding** This work was supported by National Natural Science Youth Foundation (51503007).

## Declarations

**Competing Interests** The authors declare no competing interests.

## References

- Rillig MC, Kim SW, Kim T-Y, Waldman WR (2021) The global plastic toxicity debt. *Environ Sci Technol* 55:2717–2719. <https://doi.org/10.1021/acs.est.0c07781>
- Bank MS, Hansson SV (2019) The Plastic cycle: a novel and holistic paradigm for the Anthropocene. *Environ Sci Technol* 53:7177–7179. <https://doi.org/10.1021/acs.est.9b02942>
- Rosenboom J-G, Langer R, Traverso G (2022) Bioplastics for a circular economy. *Nat Reviews Mater* 7:1–21. <https://doi.org/10.1038/s41578-021-00407-8>
- Meereboer KW, Misra M, Mohanty AK (2020) Review of recent advances in the biodegradability of polyhydroxyalkanoate (PHA) bioplastics and their composites. *Green Chem* 22:5519–5558. <https://doi.org/10.1039/d0gc01647k>
- El-Taweel SH, Khater M (2015) Mechanical and thermal behavior of blends of poly(hydroxybutyrate-co-hydroxyvalerate) with Ethylene Vinyl acetate Copolymer. *J Macromolecular Sci Part B* 54:1225–1232. <https://doi.org/10.1080/00222348.2015.1085274>
- Raza ZA, Abid S, Banat IM (2018) Polyhydroxyalkanoates: characteristics, production, recent developments and applications. *Int Biodeterior Biodegrad* 126:45–56. <https://doi.org/10.1016/j.ibiod.2017.10.001>
- Rodríguez-Fabià S, Chinga-Carrasco G (2022) Effects of a poly(hydroxyalkanoate) elastomer and kraft pulp fibres on bio-composite properties and three-dimensional (3D) printability of filaments for fused deposition modelling. *J Bioresources Bioprod* 7:161–172. <https://doi.org/10.1016/j.jobab.2022.03.002>
- Bonnenfant C, Gontard N, Aouf C (2022) Biobased and biodegradable polymers in a circular economy context: understanding quercetin and gallic acid impacts on PHBV thermal properties. *Polym Degrad Stab* 201:109975. <https://doi.org/10.1016/j.polydegradstab.2022.109975>
- Han X, Jin Y, Huang J et al (2022) Highly toughening modification of Hyperbranched polyester with environment-friendly caprolactone as end group on poly(3-hydroxybutyrate-co-3-hydroxyvalerate). *J Polym Environ* 30:3209–3217. <https://doi.org/10.1007/s10924-022-02427-z>
- Ma P, Hristova-Bogaerds DG, Lemstra PJ et al (2011) Toughening of PHBV/PBS and PHB/PBS blends via in situ compatibilization using Dicumyl Peroxide as a free-radical grafting initiator. *Macromol Mater Eng* 297:402–410. <https://doi.org/10.1002/mame.201100224>
- Ferreira WH, Silva CA, Andrade CT (2020) Improved compatibilization and shape memory properties of poly(3-hydroxybutyrate-co-3-hydroxyvalerate)/poly(ethylene-co-vinyl acetate) blends by incorporation of modified reduced graphene oxide. *Polymer* 201:122625. <https://doi.org/10.1016/j.polymer.2020.122625>
- Omri N, amine Oualha M, Brisson L et al (2020) Novel nanocomposite based on EVA/PHBV/[60]Fullerene with improved thermal properties. *Polym Test* 81:106277. <https://doi.org/10.1016/j.polymertesting.2019.106277>
- Gouvêa RF, Andrade CT (2020) Testing the effect of imidazolium ionic liquid and citrate derivative on the properties of graphene-based PHBV/EVA immiscible blend. *Polym Test* 89:106615. <https://doi.org/10.1016/j.polymertesting.2020.106615>
- Su T, Zhang R, Wang J et al (2015) Study on the poly(3-hydroxybutyrate-co-4-hydroxybutyrate)-based composites toughened by synthesized polyester polyurethane elastomer. *J Appl Polym Sci* 132. n/a-n/a <https://doi.org/10.1002/app.42740>
- Kugimoto D, Kouda S, Yamaguchi M (2019) Improvement of mechanical toughness of poly(lactic acid) by addition of ethylene-vinyl acetate copolymer. *Polym Test* 80:106021. <https://doi.org/10.1016/j.polymertesting.2019.106021>

16. Wu D, Feng Q, Li M et al (2019) Preparation and protein separation Properties of the Porous Polystyrene/Ethylene–Vinyl acetate Copolymer Blend Nanofibers membranes. *ACS Omega* 4:20152–20158. <https://doi.org/10.1021/acsomega.9b01946>
17. Kugimoto D, Kouda S, Yamaguchi M (2020) Modification of Poly(Lactic Acid) Rheological Properties using Ethylene–Vinyl acetate Copolymer. *J Polym Environ* 29:121–129. <https://doi.org/10.1007/s10924-020-01856-y>
18. Souza Junior OF, Staffa LH, Costa LC, Chinelatto MA (2019) Thermal and rheological behavior of Binary Blends of Poly(hydroxybutyrate-co-hydroxyvalerate) and poly(ethylene-co-vinyl acetate) with different vinyl acetate content. *Macromolecular Symposia* 383:1800020. <https://doi.org/10.1002/masy.201800020>
19. Zytner P, Wu F, Misra M, Mohanty AK (2020) Toughening of biodegradable poly(3-hydroxybutyrate-co-3-hydroxyvalerate)/Poly( $\epsilon$ -caprolactone) blends by in situ reactive compatibilization. *ACS Omega* 5:14900–14910. <https://doi.org/10.1021/acsomega.9b04379>
20. Zheng T, Clemons CM, Pilla S (2019) Comparative study of Direct compounding, coupling Agent-Aided and initiator-aided reactive extrusion to prepare cellulose Nanocrystal/PHBV (CNC/PHBV) nanocomposite. *ACS Sustain Chem Eng* 8:814–822. <https://doi.org/10.1021/acssuschemeng.9b04867>
21. Hu X, Su T, Li P, Wang Z (2017) Blending modification of PBS/PLA and its enzymatic degradation. *Polym Bull* 75:533–546. <https://doi.org/10.1007/s00289-017-2054-7>
22. Yan Y, Dou Q (2020) Effect of peroxide on compatibility, microstructure, Rheology, crystallization, and Mechanical Properties of PBS/Waxy starch composites. *Starch - Stärke* 73:2000184. <https://doi.org/10.1002/star.202000184>
23. Yu H-Y, Qin Z-Y, Liu L et al (2013) Comparison of the reinforcing effects for cellulose nanocrystals obtained by sulfuric and hydrochloric acid hydrolysis on the mechanical and thermal properties of bacterial polyester. *Compos Sci Technol* 87:22–28. <https://doi.org/10.1016/j.compscitech.2013.07.024>
24. Han X, Jin Y, Wang B et al (2021) Reinforcing and toughening modification of PPC/PBS blends compatibilized with epoxy terminated Hyperbranched polymers. *J Polym Environ* 30:461–471. <https://doi.org/10.1007/s10924-021-02211-5>
25. Ji D, Liu Z, Lan X et al (2013) Morphology, rheology, crystallization behavior, and mechanical properties of poly(lactic acid)/poly(butylene succinate)/dicumyl peroxide reactive blends. *J Appl Polym Sci* 131. <https://doi.org/10.1002/app.39580>
26. Wu F, Misra M, Mohanty AK (2019) Novel tunable super-tough materials from biodegradable polymer blends: nano-structuring through reactive extrusion. *RSC Adv* 9:2836–2847. <https://doi.org/10.1039/c8ra09596e>
27. Cheong W, Fellows CM, Gilbert RG (eds) (2004) Synthesis and cross-linking of polyisoprene latexes. *Polymer* 45:769–781. <https://doi.org/10.1016/j.polymer.2003.12.002>
28. Gu J, Xu H, Wu C (2014) The Effect of Benzoyl Peroxide and Divinyl Benzene on the Properties of cross-linked recycled polyolefin blends. *J Macromolecular Sci Part B* 53:1777–1785. <https://doi.org/10.1080/00222348.2013.861297>
29. Fritz H-G, Stöhrer B (1986) Polymer compounding process for controlled peroxide-degradation of PP. *Int Polym Proc* 1:31–41. <https://doi.org/10.3139/217.860031>
30. Yu H-Y, Qin Z-Y, Yan C-F, Yao J-M (2014) Green Nanocomposites based on Functionalized Cellulose Nanocrystals: a study on the relationship between Interfacial Interaction and Property Enhancement. *ACS Sustain Chem Eng* 2:875–886. <https://doi.org/10.1021/sc400499g>
31. Han X, Han Y, Jin Y et al (2022) Tailoring compatibility and toughness of microbial poly(3-hydroxybutyrate-co-3-hydroxyvalerate)/bio-based polyester elastomer blends by epoxy-terminated hyperbranched polyester. *Int J Biol Macromol* 220:1163–1176. <https://doi.org/10.1016/j.ijbiomac.2022.08.130>
32. Ding Y, Chen X, Huang D et al (2021) Post-chemical grafting poly(methyl methacrylate) to commercially renewable elastomer as effective modifiers for polylactide blends. *Int J Biol Macromol* 181:718–733. <https://doi.org/10.1016/j.ijbiomac.2021.03.139>
33. Wang Y, Wei Z, Leng X et al (2016) Highly toughened polylactide with epoxidized polybutadiene by in-situ reactive compatibilization. *Polymer* 92:74–83. <https://doi.org/10.1016/j.polymer.2016.03.081>
34. Sun X, He J, Li G et al (2013) Laminated magnetic graphene with enhanced electromagnetic wave absorption properties. *J Mater Chem C* 1:765–777. <https://doi.org/10.1039/c2tc00159d>
35. Joshi M, Butola BS, Simon G, Kukaleva N (2006) Rheological and viscoelastic behavior of HDPE/Octamethyl-POSS nanocomposites. *Macromolecules* 39:1839–1849. <https://doi.org/10.1021/ma051357w>
36. Li F, Yu H-Y, Li Y et al (2021) Soft-rigid synergistic reinforcement of PHBV composites with functionalized cellulose nanocrystals and amorphous recycled polycarbonate. *Compos Part B: Eng* 206:108542. <https://doi.org/10.1016/j.compositesb.2020.108542>
37. Shyr T-W, Ko H-C, Wu T-M, Wu T-M (2018) Crystallisation and spherulite morphology of polylactide stereocomplex. *Polym Int* 68:141–150. <https://doi.org/10.1002/pi.5708>
38. Jin Y, Ee Ge Wang, Weng Y et al (2018) The investigation of the Toughening mechanism of PHBV/PBAT with a Novel Hyperbranched Ethylenediamine Triazine Polymer based modifier: the formation of the transition layer and the Microcrosslinking structure. *J Polym Environ* 26:4158–4167. <https://doi.org/10.1007/s10924-018-1286-4>
39. Yu L, Dean K, Li L (2006) Polymer blends and composites from renewable resources. *Prog Polym Sci* 31:576–602. <https://doi.org/10.1016/j.progpolymsci.2006.03.002>
40. El-Taweel SH, Stoll B, Höhne GWH et al (2004) Stress-strain behavior of blends of bacterial polyhydroxybutyrate. *J Appl Polym Sci* 94:2528–2537. <https://doi.org/10.1002/app.21215>
41. Khonakdar HA, Morshedian J, Wagenknecht U, Jafari SH (2003) An investigation of chemical crosslinking effect on properties of high-density polyethylene. *Polymer* 44:4301–4309. [https://doi.org/10.1016/s0032-3861\(03\)00363-x](https://doi.org/10.1016/s0032-3861(03)00363-x)
42. Han X, Han Y, Jin Y et al (2023) Microcrystalline cellulose grafted hyperbranched polyester with roll comb structure for synergistic toughening and strengthening of microbial PHBV/bio-based polyester elastomer composites. *Int J Biol Macromol* 242:124608–124608. <https://doi.org/10.1016/j.ijbiomac.2023.124608>
43. Dolores Fernández M, Jesús Fernández M (2007) Thermal decomposition of copolymers from ethylene with some vinyl derivatives. *J Therm Anal Calorim* 91:447–454. <https://doi.org/10.1007/s10973-007-8552-3>
44. Sultan B-Å, Sörvik E (1991) Thermal degradation of EVA and EBA—A comparison. I. Volatile decomposition products. *J Appl Polym Sci* 43:1737–1745. <https://doi.org/10.1002/app.1991.070430917>
45. Horowitz HH, Metzger G (1963) A New Analysis of Thermogravimetric traces. *Anal Chem* 35:1464–1468. <https://doi.org/10.1021/ac60203a013>
46. Regnier N, Guibe C (1997) Methodology for multistage degradation of polyimide polymer. *Polym Degrad Stab* 55:165–172. [https://doi.org/10.1016/s0141-3910\(96\)00115-2](https://doi.org/10.1016/s0141-3910(96)00115-2)

Springer Nature or its licensor (e.g. a society or other partner) holds exclusive rights to this article under a publishing agreement with the author(s) or other rightsholder(s); author self-archiving of the accepted

manuscript version of this article is solely governed by the terms of such publishing agreement and applicable law.